Journal Pre-proof

A multifunctional nanoplatform based on MoS$_2$-nanosheets for targeted drug delivery and chemo-photothermal therapy

Yanbo Yang, Jianrong Wu, David H. Bremner, Shiwei Niu, Yu Li, Xuejing Zhang, Xiaotian Xie, Li-Min Zhu

Please cite this article as: Yang Y, Wu J, Bremner DH, Niu S, Li Y, Zhang X, Xie X, Zhu L-Min, A multifunctional nanoplatform based on MoS$_2$-nanosheets for targeted drug delivery and chemo-photothermal therapy, *Colloids and Surfaces B: Biointerfaces* (2019), doi: https://doi.org/10.1016/j.colsurfb.2019.110585

This is a PDF file of an article that has undergone enhancements after acceptance, such as the addition of a cover page and metadata, and formatting for readability, but it is not yet the definitive version of record. This version will undergo additional copyediting, typesetting and review before it is published in its final form, but we are providing this version to give early visibility of the article. Please note that, during the production process, errors may be discovered which could affect the content, and all legal disclaimers that apply to the journal pertain.

A multifunctional nanoplatform based on MoS$_2$-nanosheets for targeted drug delivery and chemo-photothermal therapy

Yanbo Yang [a,1], Jianrong Wu[a,1], David H. Bremner[b,*], Shiwei Niu[a], Yu Li[a], Xuejing Zhang[a], Xiaotian Xie[a], Li-Min Zhu[a,*]

[a]College of Chemistry, Chemical Engineering and Biotechnology, Donghua University, Shanghai, 201620, China

[b]School of Science, Engineering and Technology, Kydd Building, Abertay University, Dundee DD1 1HG, Scotland, UK

* Corresponding authors.

E-mail: lzhu@dhu.edu.cn (L.-M. Zhu) , Tel：+862167792655 (L.-M. Zhu);

[1] These authors contributed equally.

Suggested reviewers

Reviewer 1.   Xiangyang Shi

Donghua University

E-mail: *xshi@dhu.edu.cn*

Reviewer 2.   Weiguo Xu

Changchun Institute of Applied Chemistry, Chinese Academy of Sciences

E-mail: *wgxu@ciac.ac.cn*

Reviewer 3.   Gareth R. Williams

University College London

E-mail: *g.williams@ucl.ac.uk*
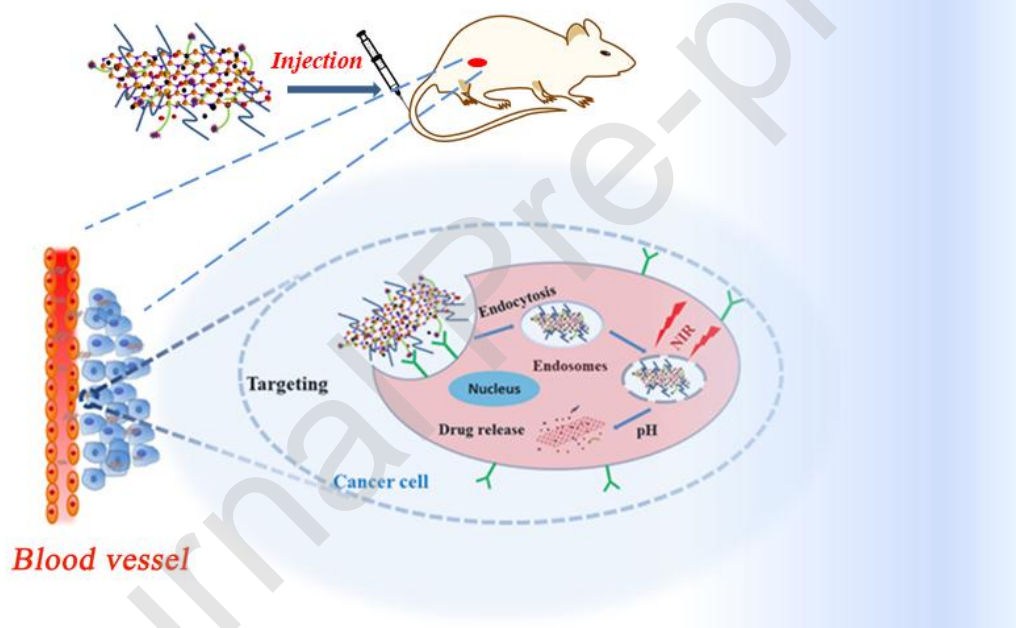
Reviewer 4.   Prof. R. Mo

State Key Laboratory of Natural Medicines and Jiangsu Key Laboratory of Drug

Discovery for Metabolic Diseases Center of Drug Discovery

China Pharmaceutical University Nanjing, 210009, China

E-mail: *rmo@cpu.edu.cn*

Graphical Abstract

Highlights

- A multifunctional platform based on melanin (Mel)-decorated, hyaluronic acid (HA)-modified MoS_2 sheets has been designed.

- The formed nanoplatform with high DOX loading capacity and exhibited pH-dependent and near-infrared laser-triggered DOX release.

2

- The synergetic effect in the enhancement of photothermal efficiency was achieved.

- The engineered HPMP@(DOX/Mel) nanoplatform exhibits excellent synergistic chemo-photothermal effect for cancer therapy.

Abstract

Synergistic tumor treatment has recently attracted more and more attention due to its remarkable therapeutic effect. Herein, a multifunctional drug delivery system based on hyaluronic acid (HA) targeted dual stimulation responsive MoS_2 nanosheets (HA-PEI-LA-MoS_2-PEG, HPMP) for active interaction with CD44 receptor positive MCF-7 cells is reported. Melanin (Mel), a new type of photothermal agent and doxorubicin (DOX) are both loaded onto the HPMP nanocomposite and can be released by mild acid or hyperthermia. The prepared HPMP nanocomposite has a uniform hydrodynamic diameter (104 nm), a high drug loading (944.3 mg.g^{-1} HPMP), a remarkable photothermal effect (photothermal conversion efficiency: 55.3%) and excellent biocompatibility. The DOX release from HPMP@(DOX/Mel) can be precisely controlled by the dual stimuli of utilizing the acidic environment in the tumor cells and external laser irradiation. Meanwhile, loading of Mel onto the surface can enhance the photothermal effect of the MoS_2 nanosheets. *In vitro* experiments showed that the HPMP@(DOX/Mel) nanoplatform could efficiently deliver DOX into MCF-7 cells and demonstrated enhanced cytotoxicity compared to that of the non-targeted nanoplatform. *In vivo* experiments in a breast cancer model of nude mice further confirmed that the HPMP@(DOX/Mel) significantly inhibited tumor growth under near infrared (NIR) laser irradiation, which is superior to any single therapy. In summary, this flexible nanoplatform, based on multi-faceted loaded MoS_2 nanosheets, exhibits considerable potential for efficient pH/NIR-responsive targeted drug delivery and chemo-photothermal synergistic tumor therapy.

*Keywords***:** MoS_2 nanosheets; Targeted drug delivery; Melanin; Synergistic therapy; Enhanced photothermal therapy.

1. Introduction

3

In recent years, the rapid development of new nanomaterials and nanotechnology has led to a research boom in effective treatment of tumors [1, 2]. Among various treatment strategies, chemotherapy has been considered as one of the most commonly used cancer treatment methods [3, 4]. However, traditional chemotherapeutic agents exhibit several disadvantages such as poor water solubility, low cancer cells uptake efficiency, severe toxic side effects on normal cells, drug resistance and non-specific delivery [5, 6]. In order to overcome the shortcomings of these chemotherapeutic agents, extensive research has been conducted on various strategies including stimuli-responsive drug-targeted delivery systems [7, 8], enhanced chemotherapeutic drug cellular uptake [9] and different combinations of therapeutic regimens [10] to improve cancer treatment efficacy and reduce side effects.

Photothermal therapy (PTT), as a minimally non-invasive treatment, has attracted widespread attention in the biomedical field in recent years [11]. PTT can effectively penetrate a few centimeters thick biological tissue and exhibit low tissue absorption [12, 13]. However, with the gradual attenuation of NIR laser in biological tissues over time, it is difficult to completely kill tumor cells by relying solely on PTT treatment [3]. Moreover, some of the photothermal agents currently reported have disadvantages such as high cost, relatively low photothermal stability, poor photothermal conversion efficiency [14] and potential toxic side effects [15]. In addition, it has been reported that PTT can not only ablate cancer cells *in situ* by hyperthermia, but the heat generated by nanoparticles can significantly improve the efficacy of chemotherapy drugs [16]. In summary, chemotherapy combined with photothermal therapy may be a promising strategy to improve cancer treatment efficiency and reduce side effects and avoid some of the drawbacks of current cancer chemotherapy and photothermal therapy because of its significant synergistic effect [17].

The so-called synergistic treatment combines some cancer treatment methods (such as chemotherapy, photothermal therapy, photodynamic therapy, etc.) to form a multifunctional nanoplatform to avoid deficiencies seen in a single therapy to improve effectiveness and optimize treatment [6, 18]. Recently, Teng et al. reported a PEG-modified MoS_2 nanosheet system for combining photothermal therapy with chemotherapy [19] and Fei et al. reported nir-laser-controlled drug release from DOX/IR-780-loaded temperature-sensitive-liposomes for chemophotothermal synergistic tumor therapy [6]. In the current study, a stimulating responsive targeted drug delivery nanoplatform was constructed for the synergistic tumor chemotherapy and photothermal therapy by

4

combining the chemotherapeutic drug DOX with the photothermal agent MoS_2 and Melanin with subsequent modification with hyaluronic acid [20-22].

Two-dimensional nanomaterials are widely used in the development of nano-devices or nanomedicines in the field of molecular biomedicine due to their ideal physical and chemical properties [23]. For example, two-dimensional transition metal disulfides (TMDCs) have attracted great interest from researchers due to their interesting electronic properties, high near-infrared absorption, and high specific surface area [19, 24-26]. As a typical representative of TMDCs, MoS_2 nanosheets have good photothermal properties and good biosafety, making them suitable candidates for next-generation photothermal therapeutics [5, 18, 26]. In particular, its constituent elements S and Mo are common biological trace elements [27, 28], thus MoS_2 is an excellent material for biomedical applications. However, the high surface energy of a few layers of nanosheets tend to inevitably stack and aggregate, which limits the application severely [29, 30]. In addition, the colloidal stability of the prepared MoS_2 nanosheet is limited, which is crucial for its application in the biomedical field [31]. In summary, it is necessary to develop a new type of MoS_2-based nanoplatforms which show good photothermal properties and bio-safety.

Our group previously conducted targeted drug delivery based on functionalized MoS_2 nanosheets and a combination of chemotherapy and photothermal therapy, but the photothermal effect of the nanomaterials requires further enhancement [30, 31]. Zhang et al. [32] reported a melanin (Mel) based liposome therapeutic diagnostic nanosystem with high biosafety and good therapeutic properties. Melanin is an endogenous bio-pigment in the human body with an intrinsic optical absorption capacity [33, 34]. The prepared Lip-Mel nanoliposomes have an ideal photothermal conversion efficiency, which can achieve complete killing of tumor cells of breast cancer-bearing mice. Consequently, due to its excellent photothermal properties and good biocompatibility, melanin is promising as a bio-safe photothermal nano-agent for photothermal ablation of tumors [35-39].

Polyethyleneimine (PEI), along with PEG, was used to modify the MoS_2 nanosheets to afford HA-functionalized MoS_2 nanosheets [28, 40-42]. The prepared HA-PEI-LA-MoS_2-PEG (HPMP) nanocarrier serves as an active targeting multifunctional nanoplatform for: (1) CD44 high expression of MCF-7 cells [43]; (2) delivering DOX and pH/NIR-responsive DOX and melanin release; and (3) synergistic chemo-enhanced photothermal therapy. Conjugating the HA to MoS_2

5

significantly enhanced the targeting efficiency in high CD44 receptor expressing MCF-7 cells. The combined loading of the chemotherapeutic drug DOX and the photothermal agent melanin in the nanocarriers enables the effective combination of chemotherapy and photothermal therapy to greatly improve the therapeutic effect on breast cancer cells. To the best of our knowledge, this is the first report of a MoS_2 nanosheet-based nanoplatform that combines multifunctional element loading for the improvement of photothermal conversion and synergistic therapy and may constitute a new class of nanoplatform for highly effective treatment of tumors.
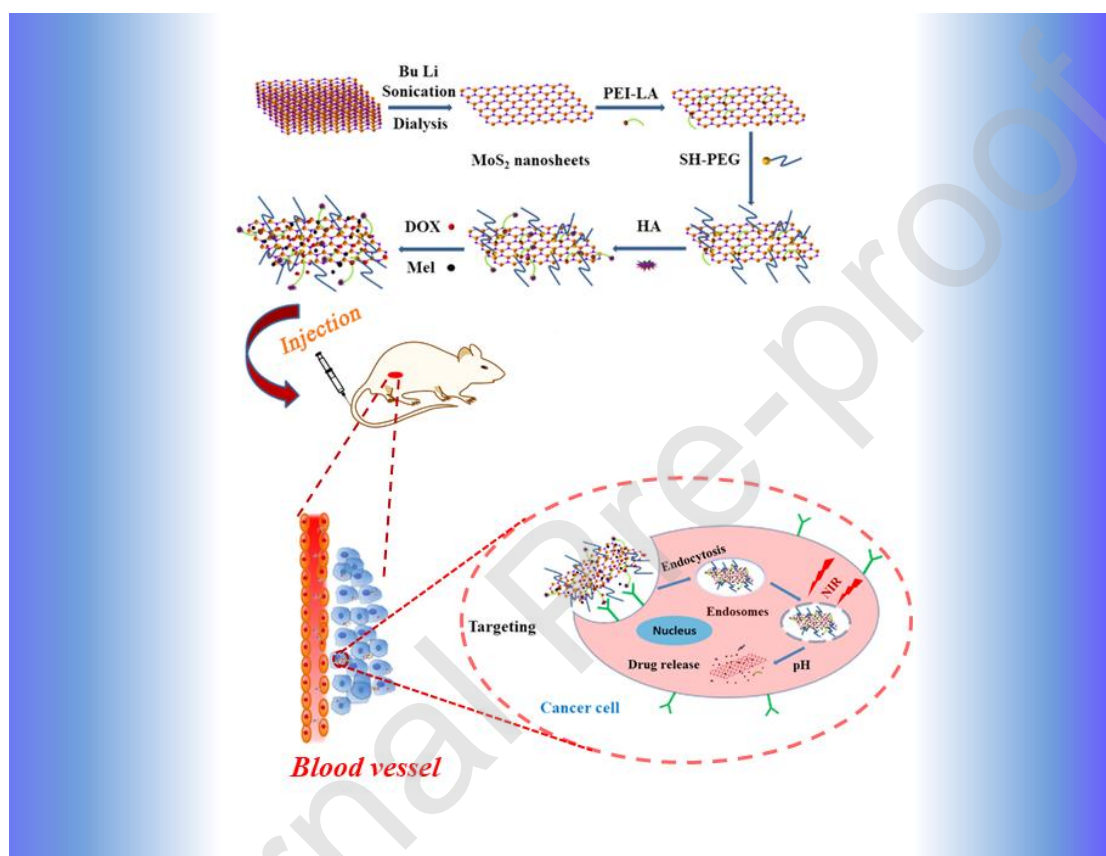
Scheme 1. Schematic illustration of the multifunctional platform based on DOX and Mel co-loaded MoS_2 nanosheets for targeted drug delivery and synergistic chemo-photothermal therapy of tumors.

2. Materials and methods

2.1. Materials

Hyaluronic acid (HA, Mw=0.5kDa) was purchased from Tianjin Hines Oppod Technology Co., Ltd. (Tianjin, China); Melanin (Mel) was obtained from Beijing Keruimai Technology Co., Ltd. (Beijing, China) and mPEG-SH (Mw=2kDa) was acquired from Shanghai Gegeen Trade Department(Shanghai,

China).Poly(ethylene imine) (PEI, Mw=25 kDa), doxorubicin (DOX), *N*-[3-(dimethyl amino)propyl]-*N'*-ethyl-carbodiimide hydrochloride (EDC), *N*-hydroxy succinimide (NHS), alpha-lipoic acid (LA), and n-BuLi solution in hexane (2.4 M) were all purchased from Aladdin Biochemical Polytron Technologies Inc. (Shanghai, China). Acetonitrile was ordered from Tianjin Hines Oppod Technology Co., Ltd. (Tianjin, China); dimethyl sulfoxide (DMSO) was purchased from Sigma-Aldrich (St. Louis, MO, USA); and 3-(4,5-Dimethyl-thiazolyl)-2,5-diphenyltetrazolium bromide (MTT), MoS_2 powder was obtained from Sinopharm Chemical Reagent Co., Ltd. 4′-6-Diamidino-2-phenylindole (DAPI) was procured from Dalian Meilun Biotech Co., Ltd. (Dalian, China). MCF-7 and L929 cell lines were obtained from KeyGEN Bio TECH Co., Ltd. (Nanjing, China).

2.2．Preparation of single-layer MoS_2 nanosheets

Single layer MoS_2 nanosheets were synthesized by using a top-down approach as reported in the literature [18]. Specifically, MoS_2 (2 g) was mixed with a solution of n-butyllithium in hexane (2 mL) and stirred for 2 d. Then, the reaction product was washed three times with an organic solvent hexane (10 mL), dispersed in purified water (30 mL) and the multilayered MoS_2 nanosheets were fully exfoliated by sonication for 90 min. The supernatant was finally collected by centrifugation at 3000 rpm/min, and then re-dispersed in water and dialyzed against a cellulose membrane (MWCO: 10000) for 3 days to obtain single layer MoS_2 nanosheets. Table S2 gives a summary of the different reaction conditions investigated and the best yield (51.6%) was obtained with 1.6 M n-buthyllithium and 90 min sonication.

2.3. Functionalization of single-layer MoS_2 nanosheets

PEI (300 mg) was dissolved in deionized water (20 mL) and the pH was adjusted to 7.4 with dilute hydrochloric acid. LA (82.4 mg) was dispersed in an organic solvent acetonitrile (20 mL). Next, EDC (191.7 mg) and NHS (115.1 mg) were sequentially added to the LA solution, stirred for 30 min, and then the PEI solution was added and stirred for 12 h. The initial product, LA-PEI, was purified by dialysis using a dialysis bag (MWCO 1000). LA-PEI (30 mg) was then dispersed in water (10 mL) and MoS_2 (2.5 mg) in water (10 mL) was added and sonicated for 15 min. After stirring at room temperature for 12 h, the resulting modified MoS_2 nanosheets were placed in a dialysis bag (MWCO 3500) and dialyzed with deionized water. The PEGylation process was conducted to introduce a PEG layer onto the surface of PEI-LA-MoS_2. mPEG-SH (25 mg) was added to a PEI-LA-MoS_2 dispersion (10 mL; 0.5 mg mL^{-1})

and, after sonicating for 15 min, the mixture was stirred for 12h and the resultant product, PEI-LA-MoS_2-SH-PEG (PMP) was obtained by centrifugation and washed several times using water (10 mL) and ethanol (10 mL).

2.4. Preparation of HA modified nanocomposites

HA (30 mg) was dispersed in purified water (20 mL) and EDC (8 mg) dissolved in purified water (10 mL) was added and sonicated for 15 min. An EDC solution (10 mL, 1 mg mL^{-1}) and an NHS solution(15 mL; 2 mg mL^{-1}) was then added, the pH adjusted to about 8.5 and the mixture was stirred at room temperature for 2 h. Finally, PMP (15 mg) was added and the reaction mixture was stirred in the dark for 12 h, the mixture was centrifuged at 10000 r/min for 15 min and the precipitate was washed 3 times with purified water to obtain HA-PEI-LA-MoS_2-PEG (HPMP).

2.5. Drug loading

The HPMP nanocarrier and the chemotherapy drug DOX were mixed in different ratios and stirred overnight in the dark at pH=7.4 and the unloaded DOX were removed by centrifugation. The amount of DOX remaining in the supernatant was determined by ultraviolet absorption spectroscopy, thereby determining the optimal mass ratio of the drug. The HPMP was mixed with the model drug DOX according to a certain ratio (1:1) and stirred overnight, and the drug-loaded composite, HPMP@DOX, was collected by centrifugation. HPMP@DOX solution (10 mL) and of Mel solution (10 mL, HPMP@DOX:Mel mass ratio of 5:1) were then mixed, stirred overnight and the precipitate was collected by centrifugation to obtain the final product HPMP@(DOX/Mel). The drug loading content of HPMP was calculated according to the following formula:

$$\text{Drug loading content of HPMP (\%)} = \frac{\text{total weight of DOX} - \text{weight of unloaded DOX}}{\text{total weight of HPMP}} \times 100\%$$

2.6. Material characterization

The morphologies and sizes of nanoparticles were measured using a JEM-2100F transmission electron microscope. Atomic force microscopy (AFM) was performed on a NanoScope IIIa from Veeco Instruments. Powder XRD patterns were performed on a Bruker D8 Advance X-ray diffractometer equipped with Cu Kα radiation (λ = 1.5418 Å). The chemical composition of the MoS_2 nanosheets was measured by X-ray photoelectron (XPS) spectroscopy (Escalab 250Xi instrument). Zeta-potential

analyses were measured using a Nano Zeta sizer instrument. The particle size distribution was measured with dynamic light scattering (DLS, Brookhaven BI-200SM). FTIR spectra were obtained using a Nicolet 6700 FTIR spectrometer (Nicolet Instruments Inc, USA). The UV-vis-NIR spectra were recorded on a UV3600 spectrophotometer (Shimadzu Corporation) and the photothermal heating effect of the MoS_2 particles were determined using an 808 nm laser (ADR-1860, Shanghai Xilong Optoelectronics Technology Co. Ltd.) at a wavelength of 808 nm.

2.7. Photothermal effects

The photothermal properties of the HPMP@(DOX/Mel) were evaluated by use of 808 nm laser irradiation (1.0 W cm^{-2}, 5 min) at different concentrations of the nanocomposite. In addition, HPMP@(DOX/Mel) at a fixed concentration of 1.0 mg mL^{-1} was irradiated with various 808 nm laser power intensities, with HPMP being used as a control. Furthermore, in order to test photostability, the HPMP@(DOX/Mel) nanocomposites (200 μL; 1.0 mg mL^{-1}) were irradiated for 10 min(power density: 1.0 W cm^{-2}). The experiment was carried out four times in succession and the temperature of the solution was simultaneously recorded every 5s using an infrared (IR) thermal imaging system. Also, the temperature of different samples was recorded using an FLIR Automation & Science Camera. The photothermal transduction efficiency of HPMP@(DOX/Mel) was measured by use of previously reported methodology [44] with some modification as shown in equations (2) and (3):

$$\eta_T = \frac{hA(T_{Max} - T_{Surr}) - Q_D}{I(1 - 10^{-A_{808}})}(2) \qquad\qquad \tau_s = \frac{m_D C_D}{hA}(3)$$

where h is the heat transfer coefficient, A is the surface area of the container, T_{max} is the equilibrium maximum temperature, T_{surr} is the surrounding ambient temperature, Q_D is heat absorption of the quartz cell, I is the laser power (250 mW), A_{808} is the absorbance of HPMP@(DOX/Mel) at 808 nm, τs is the system time constant and m_D and C_D are the mass (0.2 g) and the heat capacity (4.2 J g^{-1})of deionized water, respectively.

2.8. In vitro drug release

HPMP@(DOX) (2 mL;1 mg mL^{-1}) dissolved in a PBS solution (pH 7.4 or pH 5.0) was put into a dialysis bag (Mw=6 KDa) and dialyzed in a beaker of PBS solution (50 mL) with different pH values with or without 808 nm laser irradiation (1 W cm^{-2}). A sample (1 mL) of the PBS solution in the beaker

was taken at different time points and an equal amount of PBS solution was added. The cumulative release of drug DOX was measured at 480 nm using an ultraviolet spectrophotometer.

2.9. Cell culture and cytotoxicity assays in vitro

MTT was performed to assess the cytotoxicity of HPMP to normal cells (L929) and cancer cells (MCF-7). First, MCF-7 and L929 cells were treated with DMEM containing 1% penicillin and 1% streptomycin. Cells were seeded into 96-well plates at a density of 1×10^4 cells per sample. Different concentrations (1.5, 3, 6, 12 and 24 µg mL^{-1}) of HPMP were then added to both cells and incubated for 24 h at 37 °C in a 5% CO$_2$ incubator. Next, MTT reagent (20 µL; 5 mg mL^{-1}) was added, and after further incubation for 4 h, the supernatant was taken out, and the MTT-formazan produced in the cells was dissolved in an organic solvent DMSO (150 µL) for 15 min. Finally, the solution optical density was measured at 570 nm using a microplate reader (MULTSIKAN MK3, Thermo Fisher).

To evaluate the potential of *in vitro* chemistry-photothermal synergistic therapy, MCF-7 cells were seeded in 96-well plates (density: 1×10^4), and cultured in an incubator at 37 °C, 5% CO$_2$ for 24 h. Next, without/with the presence of 808 nm laser (power density: 1.0 W cm^{-2}, 10 min), MCF-7 cells were incubated with various concentrations (1.5, 3, 6, 12, 24 µg mL^{-1}) of free DOX，HPMP@DOX, HPMP@DOX+NIR, HPMP@Mel+NIR, PMP@(DOX/Mel)+NIR, and HPMP@(DOX/Mel)+NIR for 36 h in DMEM. Then, after incubating for 4 h by adding MTT solution (20 µL, 5 mg mL^{-1}), the supernatant was taken out, and MTT-methane produced by living cells was dissolved in an organic solvent DMSO (200 µL) for 20 min. Finally, the absorbance of each well solution was measured at 570 nm on a microplate reader (MULTSIKAN MK3, Thermo Fisher).

2.10. In vitro cellular uptake

Tumor cell targeting performance of synthetic nanomaterials was studied by using confocal laser scanning microscopy (CLSM, Jena, Germany). MCF-7 cells (CD44 receptor positive) were seeded into 24-well plates at a density of 1×10^5 cells per well and cultured for 24 h. All cells were treated with free DOX, PMP@(DOX/Mel), HPMP@(DOX/Mel) and HPMP@(DOX/Mel) with laser irradiation for 30 min at an equivalent DOX concentration of 5.0 µg mL^{-1} for 4 h followed by washing the cells with PBS. After the cells were further cultured for 2 h, they were then washed and fixed with 4% formaldehyde solution (time: 30 min). Cancer cell nuclei were labeled with DAPI

and cell images were recorded by CLSM (,.

2.11. In vivo infrared thermal imaging

For thermal imaging in mice, first, nude mice bearing MCF-7 tumors were anesthetized with pentobarbital (1%) and injected with HPMP@DOX or HPMP@(DOX/Mel) solution (1.0 mg mL^{-1}) into nude mice containing MCF-7 tumors by intravenous injection. A saline (200 µL) group was used as a control group. Next, mouse tumor sites were irradiated with 808 nm laser for *in vivo* thermography (0.8 W cm^{-2}, 8 min) and the temperature and IR thermal images of tumor sites were recorded at different time points using FLIR Automated & Scientific Camera.

2.12. In vivo experiments

Animal experiments were performed following protocols approved by the Institutional Animal Care and Use Committee of Nanjing Medical University and all the animals were treated in compliance with the Nanjing Maternity and Child Health Care Hospital's guidelines. 4-6 week old nude mice were obtained from Nanjing Pengsheng Biotechnology Co., Ltd., and each mouse was inoculated with 1 x 10^6 MCF-7 cells by subcutaneous injection. When the tumor size of the mice after MCF-7 cell inoculation was 50 mm^3, the experimental mice were randomly divided into 5 groups of 3 each. Next, each mice was injected intravenously: saline (control), free DOX (3 mg kg^{-1}), HPMP@(DOX/Mel) (chemotherapy), PMP@(DOX/Mel) + NIR or HPMP@(DOX/Mel)+ NIR (synergistic therapy). The tumor regions of the NIR groups were irradiated with 808 nm laser energy (1.0 W cm^{-2}; 5 min) on the second day (at 24 h post-injection). Body weight and tumor volume were measured every 2 days after irradiation and the tumor volume was calculated according to the formula $V = W^2 \times L/2$, where W and L are the width and length diameters, respectively.

2.13. Histological analysis

After culturing the experimental mice for 25 days, representative mice of the five groups were killed. The tumor and the main organs of the body (heart, lung, spleen, liver and kidney) were excised from the experimental mice and a 4% paraformaldehyde solution was selected as a fixative and processed into paraffin sections. Finally, the main organs were stained with H&E and the tumor tissues were stained with H&E and TdT-mediated dUTP Nick-End Labeling (TUNEL) for histopathology analysis.

11

2.14. Statistical analysis

Every experiment was performed three times and the results are presented as the mean SE ± SD. All statistical analyses were performed with Graph Pad Prism software and the significance of the data for all tests were analyzed using Student's t test: *P < 0.05, **P < 0.01 and ***P < 0.001.

# 3. Results and discussion

## 3.1. Synthesis and characterization of nanocomposites

Scheme S1 demonstrated the preparation strategy for HPMP nanoparticles (Supporting Information). Single-layered MoS_2 nanosheets were synthesized by chemical exfoliation from multilayered MoS_2 as described previously [18] which was optimized by varying the reaction conditions as shown in Table S2. The highest yield obtained reached 51.6%, which is close to the reported research [45]. As shown in Scheme S1a and S1b, LA-PEI was prepared by simple amide coupling following the previously reported method [18]. Surface modification of the prepared MoS_2 nanosheets by PEI via thiol reaction where the sulfur moiety of the LA binds to the defect regions in the MoS_2 nanosheets. Similarly, thiolated PEG is also grafted onto the surface of PEI-LA-MoS_2 to form PEI-LA-MoS_2-PEG (PMP) (Scheme S1c). The PMP and HA were mixed and sonicated and then EDC and NHS were added for activation and HA was grafted onto the surface region of the PMP by forming an amide bond between the carboxyl group of the HA and the amino group of the PMP to obtain nanocomposite HPMP (Scheme S1d).

It can be seen from the TEM picture that the size of MoS_2 nanosheets is ~50-80 nm (Fig. 1a). The XPS data of MoS_2 show characteristic peaks at 517 eV (Mo3s), 413 eV (Mo 3p1), 359 eV (Mo 3p3), 233eV (Mo 3d,) 64 eV (Mo 4s) and 38 eV (Mo 4p)(Fig. 1b). These XPS data are similar to other literature reports on MoS_2 slices [46]. AFM imaging shows that the MoS_2 nanosheets have a thickness of about 1.8-2.2 nm, about 2 to 3 layers (Fig. 1c and d) [28]. The peaks at $2\theta=14.28^{\circ}$, 33.54° and 58.96° were correspond to the (002), (100) and (110) planes of the hexagonal MoS_2, respectively (Fig. 2a) [3]. Several distinct diffraction peaks of the sample matched with the standard patterns of the hexagonal MoS_2 (JCPDS 37–1492), indicating successful synthesis of MoS_2 nanosheets [47]. The fabricated nanoplatform was further confirmed by FT-IR spectra (Fig. 2b) where the characteristic absorptions of PEI-LA-MoS_2 at 3415 cm^{-1}, 2933cm^{-1} and 1642 cm^{-1} indicated the presence of -OH strand, CH$_2$ asymmetric strand bending mode of the amino group (-NH$_2$). Also, the peaks at 2856 cm^{-1} and 1628 cm^{-1} in HPMP can be attributed to the C-H strand the carbonyl-amide (-CO-NH-) vibration of HA. Formation of the stable

12

nanocomposites was further confirmed by DLSanalysis (Fig. 2c). After grafting the target molecule HA on the surface of MoS_2 nanosheets by LA-PEI, the hydrodynamic diameter of the resulting HPMP is 104 nm, which is increased compared to the bare MoS_2 (80 nm). In addition, HPM without mPEG-SH modification and mPEG-SH modified HPMP were formulated into a certain concentration of aqueous solution to stand at room temperature. The results showed that HPMP had higher colloidal stability, and HPMP was still well dissolved in deionized water without being deposited after standing for 24 h (Fig. S1). Moreover, the zeta potential of the MoS_2 nanosheets and HA was about -24 mV and -16 mV, respectively (Fig. 2d). Next, the LA-PEI was grafted on the surface of the MoS_2 nanosheets by forming a disulfide bond, and the zeta potential of the particles was changed from -24 mV to +6 mV. The HA was further grafted by the formation of an amide bond, and the zeta potential of the HPMP nanoparticles was changed to -23 mV. In summary, the zeta potential change of the nanoparticles indicates that the targeting molecule HA is successfully bound to the surface of the MoS_2 nanosheets. In addition, the successful loading of DOX and melanin on the nanocomposite HPMP was demonstrated by UV absorption spectroscopy (Fig. 3a and 3b). DOX exhibits an adsorption peak at 480 nm, which is also evident in the spectrum of HPMP@DOX. Melanin shows adsorption peaks at 258 nm and 369 nm, which are also evidented in the absorption spectrum of HPMP@(DOX/Mel), demonstrating the successful loading of melanin onto the nanocomposite HPMP@DOX.
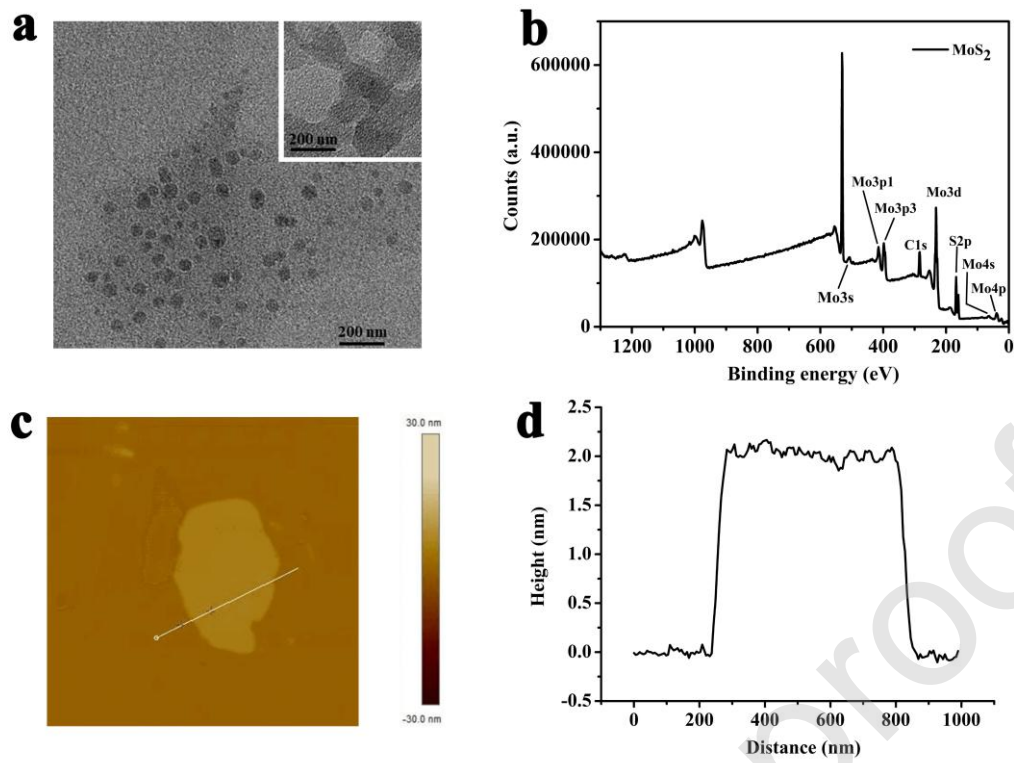
Fig. 1. (a) TEM image of MoS$_2$ nanosheets; (b) XPS survey spectrum of MoS$_2$; (c) AFM images of the MoS$_2$ nanosheets and (d) the corresponding AFM height profile.
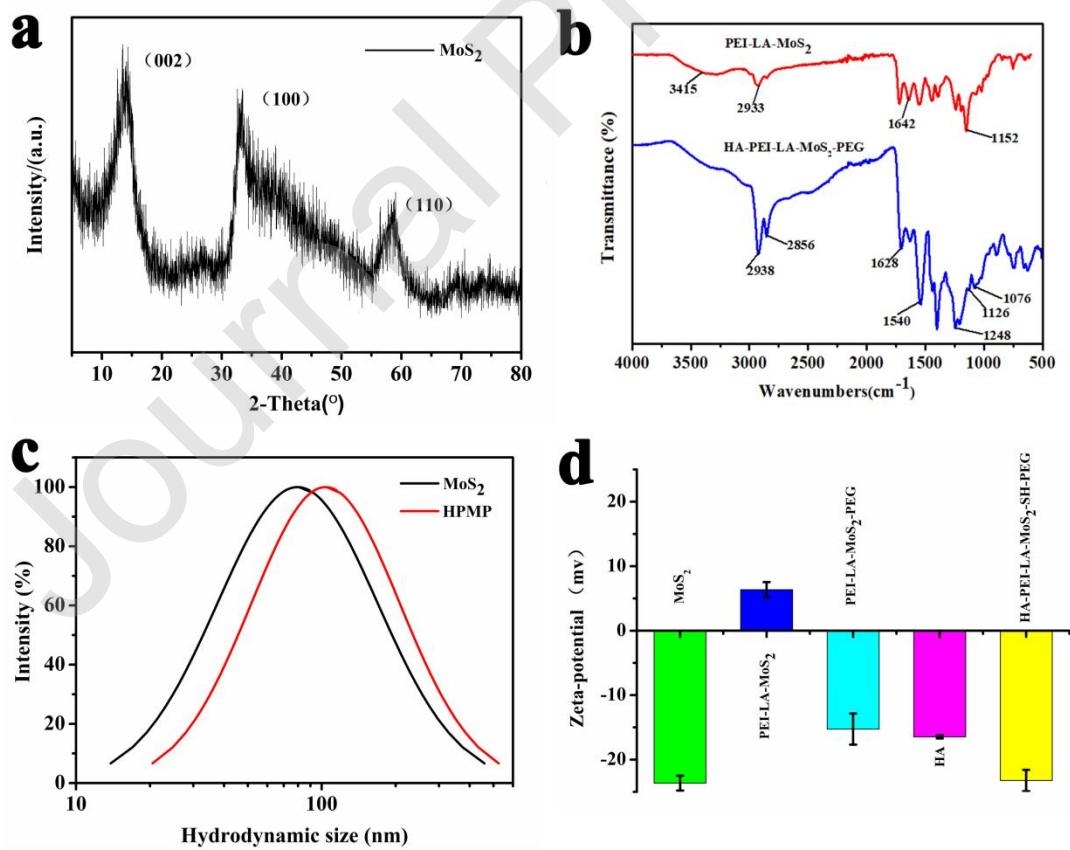
Fig. 2. (a) XRD pattern of the MoS_2 nanosheets; (b) Infrared spectroscopy analysis of PEI-LA-MoS_2 (red) and HPMP (blue); (c) Hydrodynamic diameters of MoS_2 (black) and HPMP (red); (d) The zeta potential changes of nanoparticles are functionally modified to form HPMP processes.

3.2. Photothermal activity

First, the photothermal efficiency of HPMP@(DOX/Mel) and HPMP nanocomposites were determined. The HPMP@(DOX/Mel) composite was suspended in water at different concentrations and was irradiated with a 1.0 W cm^{-2} 808 nm laser. As shown in Fig. 3c, the temperature of the HPMP@(DOX/Mel) aqueous solution increased with the concentration of the nanoparticles and the laser irradiation time. When the concentration of the HPMP@(DOX/Mel) nanocomposites was 0.8 mg mL^{-1}, the temperature reached 52 °C within 300 s, indicating that the nanoparticles HPMP@(DOX/Mel) had a good photothermal effect. Also, the temperature increase was found to be directly related to laser power for HPMP@(DOX/Mel) aqueous solutions (Fig. 3d). Furthermore, the photostability of HPMP@(DOX/Mel) (1.0 mg mL^{-1}) was also examined during four 1.0 W cm^{-2} laser irradiation on/off cycles and almost no noticeable attenuation could be observed in the temperature-time curve after the cycles (Fig. 3e). This implied that the HPMP@(DOX/Mel) nanocomposites had excellent photothermal stability and were suitable for photothermal ablation of tumors. More importantly, the temperature elevation for the HPMP@(DOX/Mel) nanoplatform was superior to that of HPMP under the same conditions, indicating a synergetic effect in the enhancement of photothermal efficiency due to the loading of Mel (Fig. 3f). Also, the photothermal conversion efficiency (η) of HPMP@(DOX/Mel) was calculated to be 55.3% according to the method reported in the literature (Fig. 3g and 3h) [44].
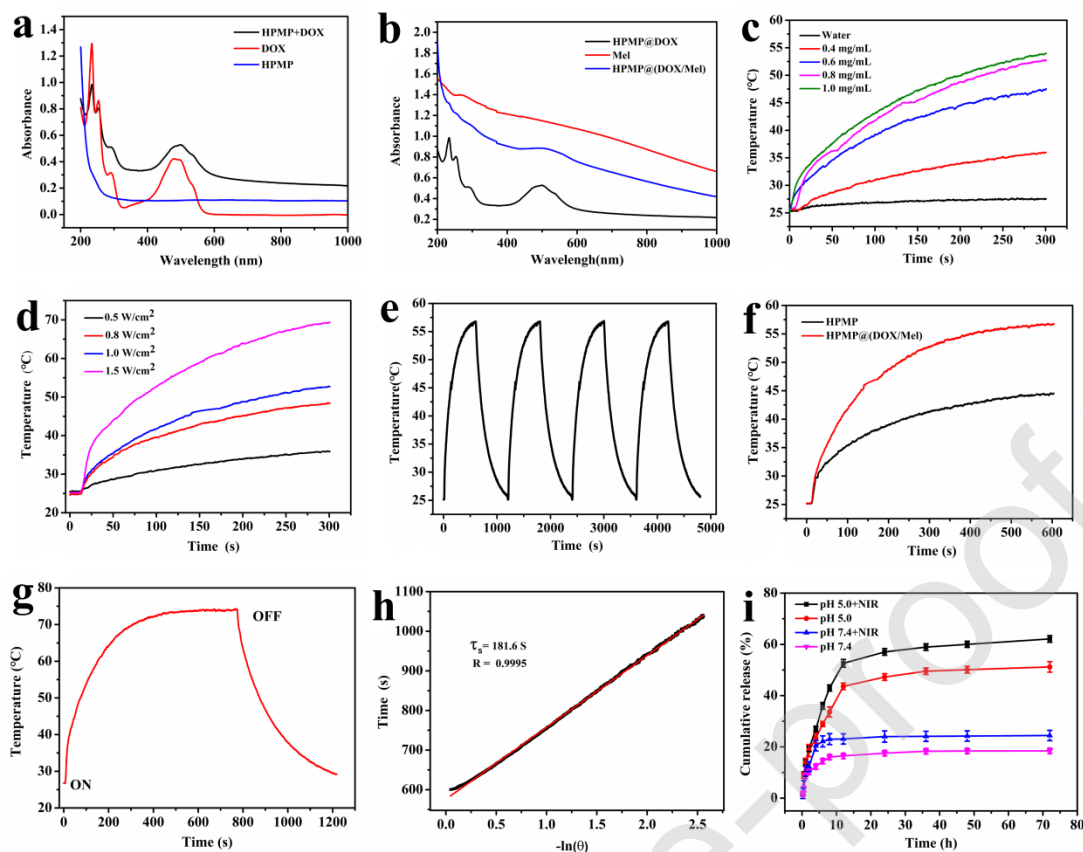
Fig.3. (a) UV-Vis spectral analysis before and after HPMP loading DOX. (b) UV-Vis spectral analysis before and after HPMP@DOX loading of Mel. (c) Temperature increase of different concentrations of HPMP@(DOX/Mel) dispersions were irradiated with a 1.0 W cm^{-2} laser for 5 min. (d) Temperature increase of an HPMP@(DOX/Mel)dispersion (1.0 mg mL^{-1}) at different laser power densities for 5 min. (e) Temperature plot of an HPMP@(DOX/Mel) dispersion (1.0 mg mL^{-1}) irradiated by an 808 nm laser (1.0 W cm^{-2}) for four on-off cycles. (f) Temperature increase of the nanocarrier before and after loading of Mel (1.0 W cm^{-2}, 10 min). (g) Plot of temperature vs time for the HPMP@(DOX/Mel) during laser irradiation (808 nm, 1.5 W cm^{-2}) and cooling (laser off) stages. (h) Linear time data versus ln(θ) obtained from the cooling period with laser off. (i) Release profiles from HPMP@DOX with or without 1.0 W cm^{-2} 808 nm laser (irradiation times: 1h, 4h, 8h, 12h, 24h, 36h, 48h; pH 7.4 and 5.0).

3.3. In vitro pH/NIR -triggered drug release

The optimum mass ratio of DOX to HPMP was first investigated at pH 7.4 and it was seen that the loading of DOX reached a maximum when the nanocomposite HPMP was mixed with DOX in a ratio of 1:1. Thus, DOX (944.3 mg) could be loaded onto HPMP (1 g) (Table S1). The *in vitro* drug release of

HPMP@DOX was then investigated in PBS buffers at pH 7.4 and 5.0 with and without 808 nm laser irradiation. As shown in Fig.3i, the DOX released from the HPMP@DOX was less than 5% at pH 7.4 after 1 h, however, the release of DOX exceeded 12% at pH 5.0 after 1 h. These results may be due to the decrease of the hydrophobic interaction and electrostatic interaction forces between the DOX and HPMP nanocomposites, which can dramatically accelerate DOX release. Next, the influence of laser irradiation on HPMP@DOX drug release was further studied (Fig. 3i). At pH 5.0, without NIR laser irradiation, HPMP@DOX released about 24.8% of DOX within 6 h, however, when irradiated with a 1.5 W cm^{-2} 808 nm laser at pH 5.0, the amount of DOX released from HPMP@DOX increased to 31.6%. In summary, the NIR-triggered nanoparticle photothermal effect could accelerate the release of DOX drugs in HPMP@DOX. This may be due to the high temperatures generated by the MoS$_2$ nanosheets causing vibration of the HPMP nanocomposite, thereby reducing the interaction between DOX and the nanoplatform [18, 47]. Taking into account that laser irradiation can be adjusted accurately, the pH/NIR multiple-stimuli-responsive HPMP@(DOX/Mel) are expected to be applied to "on demand" chemotherapy of cancer.

3.4. In vitro cell viability

It is well known that the cytocompatibility of nanocarriers is critical for an ideal drug delivery system. Therefore, the cell viability of HPMP-treated MCF-7 and L929 cells was investigated by MTT. After incubation for 48 h with different concentrations of HPMP nanocomposites, the overall viability remains above 95% at the highest HPMP concentration tested, confirming that the HPMP possess an excellent cytocompatibility in the given concentration range (Fig. S2).

The therapeutic efficacy was evaluated by comparing cell viabilities after incubating L929 and MCF-7 cells with culture medium, free DOX, HPMP@DOX, HPMP@Mel with NIR laser irradiation, HPMP@DOX with NIR laser irradiation, and HPMP@(DOX/Mel) with or without NIR laser irradiation (Fig. 4a and 4b). Compared to the separate free DOX treatment group, the cell viability of L929 cells in the HPMP@DOX treatment group (DOX concentration: 1.5 μg mL^{-1}) was significantly increased. However, for MCF-7 cells, the results were reversed, which indicated that the nanocarrier loading of DOX enhanced the chemotherapeutic effect on tumor cells. It was also found that under near-infrared light irradiation, the cell viability of both groups treated with HPMP@Mel decreased and the activity of the MCF-7 cell group was the lowest, indicating that the nanocomposite loaded with Mel had a good

17

photothermal treatment effect on tumor cells. It is worth noting that the external stimulation with near-infrared light can not only achieve the purpose of photothermal treatment to kill cancer cells, but also promotes the release of the chemotherapeutic drug DOX from the nanocarriers, thereby enhancing the effect. This can be attributed to the thermal energy generated by near-infrared light stimulation that disrupts the π-π stacking effect between DOX and the nanocarrier HPMP [48].

Finally, under the conditions of near-infrared light irradiation, the cell viability of the two groups of cells treated with (PMP@(DOX/Mel), HPMP@DOX and HPMP@(DOX/Mel) was studied. MCF-7 cells treated with HPMP@(DOX/Mel) showed the lowest cell viability compared to the two groups treated with PMP@(DOX/Mel) and HPMP@DOX. This indicated that the loading of Mel significantly enhanced the synergistic therapeutic effect of photothermal therapy and chemotherapy to tumor cells and the synergistic therapeutic effect of tumor cells is significantly better than any single therapy such as chemotherapy or photothermal therapy alone. In addition, the loading of the targeting molecule hyaluronic acid allowed the nanocomplex to be selectively taken up by tumor cells. All the results showed that the prepared nanocomposite HPMP@(DOX/Mel) can effectively concentrate photothermal therapy and chemotherapy into a multifunctional drug delivery system, greatly improving the killing effect on tumor cells.
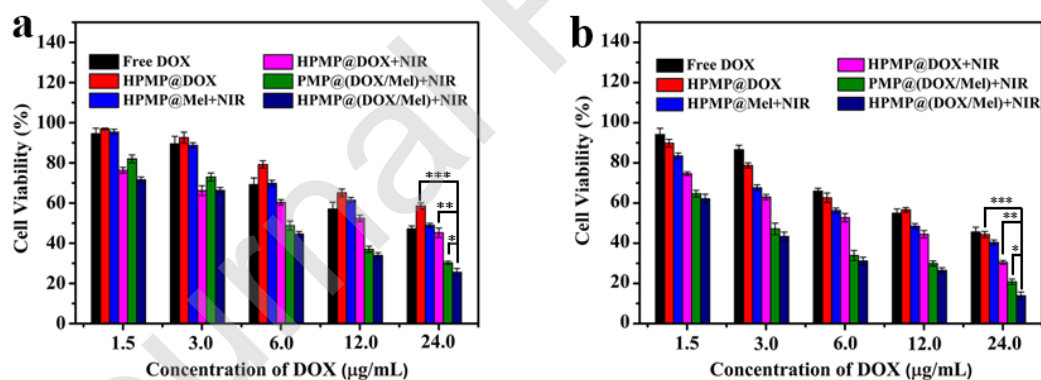

Fig. 4. Relative cell viability of (a) L929 cells and (b) MCF-7 cells incubated with DOX or the different nanocomposite with a DOX concentration of 1.5–24 μg mL^{-1} for 48 h. *P < 0.05, **P < 0.01, and ***P < 0.001.

3.5. Cellular uptake

The active targeting effect of HA-modified nanocomplexes to cancer cells was studied using CLSM. MCF-7 cells (CD44 receptor positive) were selected as model cancer cells and the free DOX treated

group was used as a control. As shown in Fig. 5, MCF-7 cells treated with HPMP@(DOX/Mel) (targeting group) showed brighter DOX fluorescence compared to PMP@(DOX/Mel) (non-targeted group) cells, indicating that the uptake behavior of HPMP@(DOX/Mel) in MCF-7 cells is associated with CD44 receptor-mediated endocytosis pathway. Also, MCF-7 cells treated with HPMP@(DOX/Mel) under near-infrared laser irradiation had a stronger DOX fluorescence than other treatment groups and can be attributed to the local high temperature-induced cell membrane damage caused by MoS_2 and Mel under near-infrared laser irradiation, which increases the uptake of nanocomplexes by the MCF-7 cells [49]. The quantitative flow cytometry measurement further confirmed that the cellular uptake of the nanoplatform (Fig. 6). It is concluded that HA-modified nanocomplexes can specifically deliver DOX to MCF-7 cells via the CD44 receptor-mediated endocytic under NIR laser irradiation, thereby increasing the cancer chemotherapy-photothermal synergistic treatment effect.
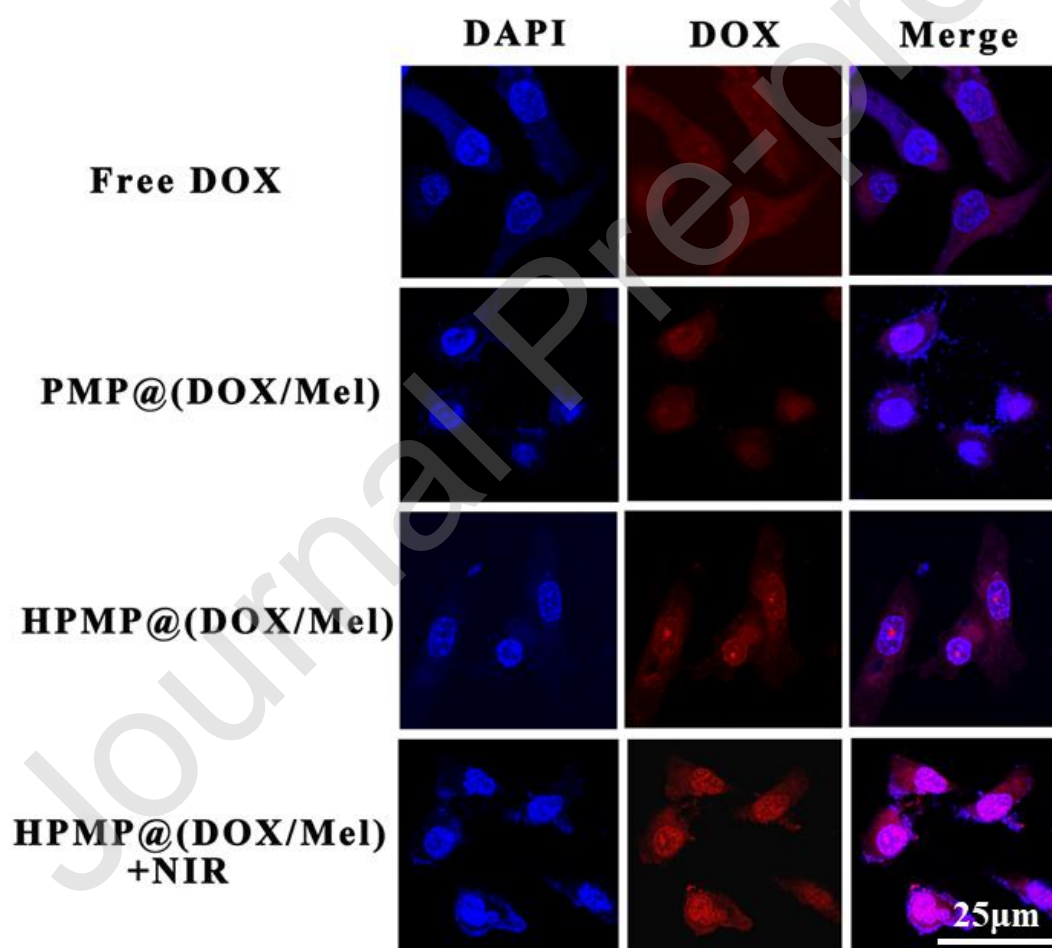
Fig. 5. Confocal microscope images of MCF-7 cells treated with free DOX, PMP@(DOX/Mel), HPMP@(DOX/Mel) and HPMP@(DOX/Mel) with laser irradiation for 30 min at an equivalent DOX concentration of 5.0 μg mL^{-1} for 4 h. Scale bar: 25 μm.
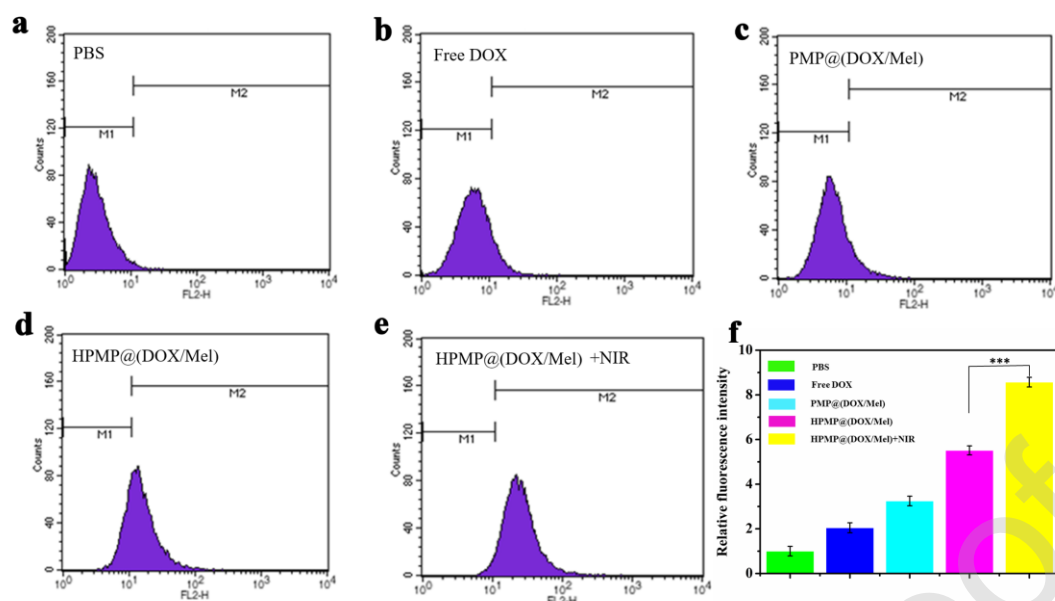
Fig. 6. Flow cytometry data for (a) untreated MCF-7cells (b) Free DOX or (c) PMP@(DOX/Mel) (d) HPMP@(DOX/Mel) (e) HPMP@(DOX/Mel) +NIR. (f) The relative fluorescence intensity values calculated from panels (a–e). The data are represented as mean ± S.D. (n = 3). ***P < 0.001.

3.6. Antitumor effect in vivo

Encouraged by the attractive ability of Mel-triggered enhanced photothermal conversion efficiency of nanoparticles and the dual-responsive drug release shown above with HPMP@(DOX/Mel), the *in vivo* photothermal performance and antitumor effects of HPMP@(DOX/Mel) were investigated. Fig. 7a shows the temperature change of the tumor region during the 808 nm laser irradiation of the tumor-bearing mice of the different treatment groups as recorded by a thermal camera. For mice injected with just saline, only a slight temperature change was observed at the tumor site. For the HPMP@DOX treated mice, the temperature of the tumor site reached 43 °C within 8 min 808 nm laser irradiation. Compared with the above two groups, the temperatures of the HPMP@(DOX/Mel) group were raised to 48 °C (Fig. 7b), which was sufficient to ablate the tumor tissue. From the photographs of the tumors excised from the experimentally treated mice (Fig. 7c), it can be seen that the size of the tumors injected with HPMP@(DOX/Mel) is obviously smaller than that of the other treatment groups under near-infrared light. Meanwhile, the relative tumor volume (V/V$_0$) curves of tumor-bearing mice after different treatments are shown in Fig. 7d. In particular, compared with the other treatment groups, the injection of HPMP@(DOX/Mel) group under the near-infrared laser irradiation can effectively inhibit the growth of mouse tumors, indicating that the killing effect on cancer cells is significantly enhanced due to the

20

synergistic effect of chemotherapy and photothermia and the active targeting of HA. Interestingly, the chemotherapy groups (HPMP@(DOX/Mel), free DOX, or photothermal therapy (HPMP@Mel with laser irradiation) also inhibited tumor cell growth to some extent, but these were not as effective as the synergistic treatment group. Also, the killing effect of HPMP@DOX and NIR irradiation groups on tumor cells is not as good as that of the HPMP@(DOX/Mel) plus NIR irradiation group, indicating the loading of melanin significantly improves the effectiveness of the photothermal ablation. In addition, the body weight of the mice in the HPMP@(DOX/Mel) plus NIR irradiation group was well maintained, similar to the other groups, indicating that the HPMP@(DOX/Mel)NPs had very little negative side effects (Fig. 7e).
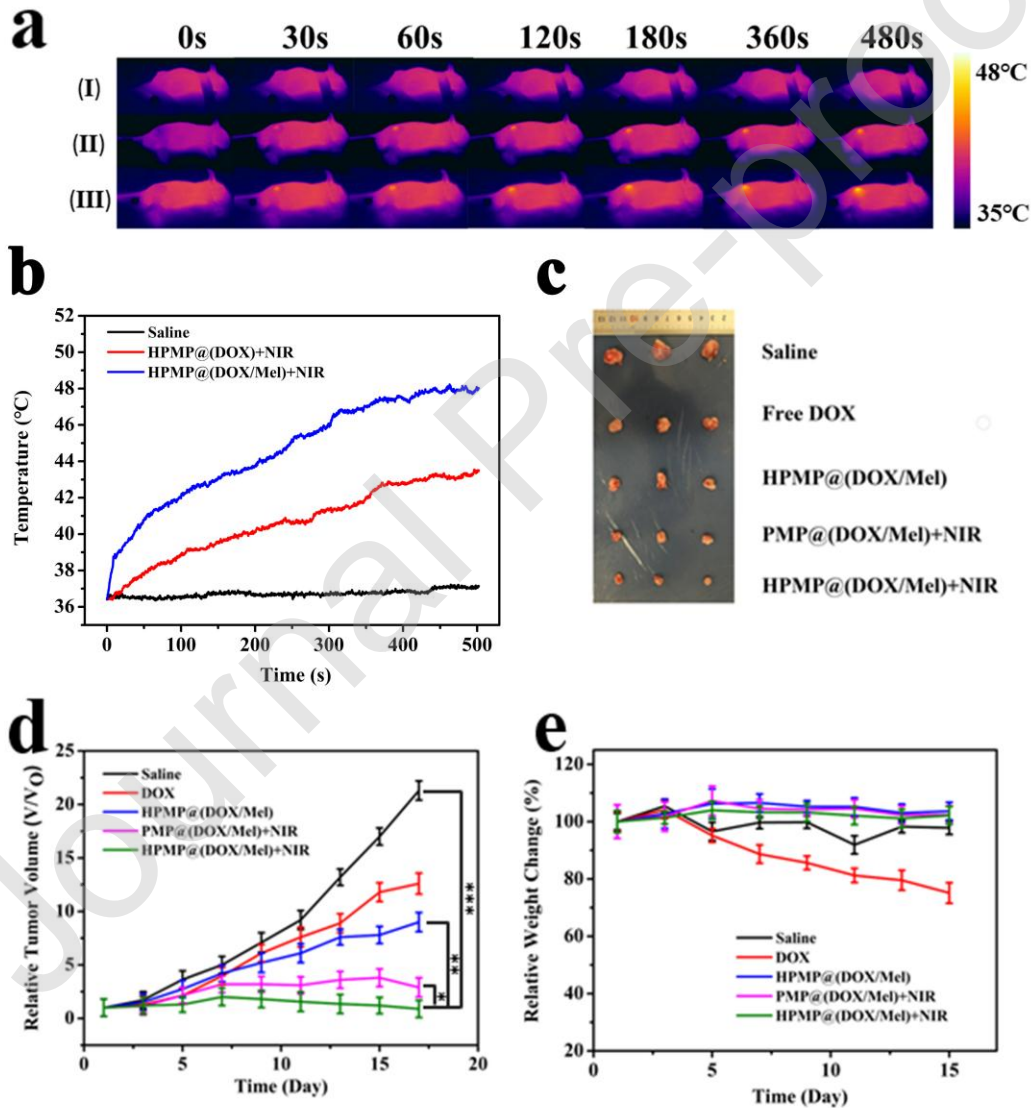

Fig.7. (a) Photothermal images ((I). Saline; (II). HPMP@(DOX)+NIR; (III). HPMP@(DOX/Mel)+NIR) and (b) corresponding temperature profile of tumor sites over time after treatment of MCF-7 tumor-bearing mice with Saline、

HPMP@(DOX) or HPMP@(DOX/Mel) under 808 nm laser irradiation ($0.8 \ W \ cm^{-2}$). (c) Photographs of the tumors dissected from the mice at the end of each treatment. (d) Relative tumor growth curves of the five groups after various treatments (n = 5); *P < 0.05, **P < 0.01, and ***P < 0.001. (e) Body-weight curves of mice after different treatments.

3.7. Histology analysis

Histology analysis, including hematoxylin and eosin (H&E) staining and terminal deoxynucleotidyl transferase-mediated dUTP nickend labeling (TUNEL) in tumor tissues were conducted (Fig. 8a). As shown by the H&E stained tumor sections, the HPMP@(DOX/Mel) + laser group has only a small fraction of purple-blue (normal nucleus) and more deformed nuclei (nuclear pyknosis, nuclear rupture and nuclear lysis), indicating that cancer cells are highly apoptotic. From the results of the TUNEL measurements, the dark brown nuclei in the HPMP@(DOX/Mel) + laser group indicate apoptosis-positive cells. In summary, synergistic chemo-photothermal treatment assisted by HPMP@(DOX/Mel) shows a good therapeutic effect *in vivo*. Furthermore, the main organs (heart, lung, liver, spleen, and kidney) of the mouse were taken out after the treatment and sectioned for H&E staining examination (Fig. 8b). No significant histopathological damage was shown in these tissues, demonstrating that the synergistic treatment had little adverse effects on the normal organs of the mice, which confirmed the negligible long-term toxicity of the material.
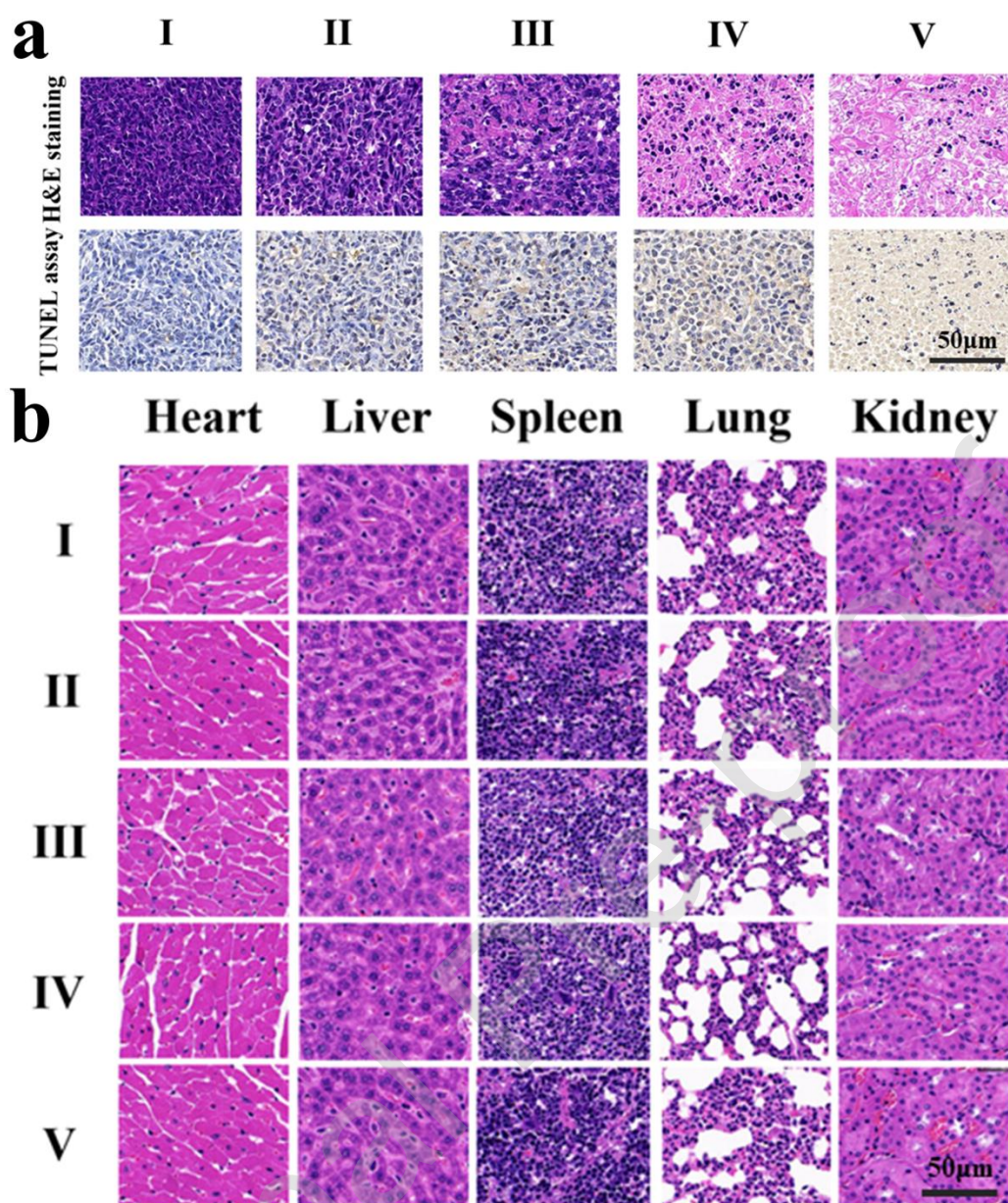
Fig.8. (a) H&E staining and TUNEL staining of tumor sections after various treatments. (b) Representative H&E sections of major organs (heart, liver, spleen, lung and kidney) of MCF-7 tumor-bearing nude mice after various treatments (I. Saline; II. Free DOX ; III. PMP@(DOX/Mel)+NIR; IV. HPMP@(DOX/Mel);V. HPMP@(DOX/Mel) + NIR. All the scale bars are 50 μm.)

4. Conclusions

A new multifunctional HPMP@(DOX/Mel) nano-platform was successfully synthesized and the synergistic chemo-photothermal therapy was studied. First, the MoS_2 nanosheets were functionalized with biodegradable hyaluronic acid (HA) in the presence of polyethyleneimine (PEI), while the MoS_2

23

nanosheets were modified with mPEG-SH to achieve better biocompatibility under physiological conditions. The chemotherapeutic drug DOX and the photothermal agent melanin were then simultaneously loaded onto the HPMP nanocarrier to study the effect of synergistic chemo-photothermal therapy. The prepared HPMP nanocomposite has a uniform particle size (104 nm), a high drug loading (944.3 mg.g^{-1} HPMP), excellent biocompatibility and good thermal properties (photothermal conversion efficiency: 55.3%). The resulting versatile platform showed the following characteristics: (1) high load efficiency of DOX; (2) the payload of endogenous bio-pigment melanin greatly improved the photothermal conversion effect of the nanocomposite HPMP; (3) the nanocomplex was specifically delivered into MCF-7 cells by an endocytosis pathway mediated via the HA-targeted CD44 receptors; (4) the loaded chemotherapeutic drug DOX showed a significant double-stimulated response release when irradiated with light at 808 nm in the weakly acidic environment of tumor cells. Overall, the results of animal experiments indicated that the chemical photothermal synergy therapy of HPMP@(DOX/Mel) had an excellent therapeutic effect compared to single therapy. Therefore, this new multifunctional nano-platform is promising as a multi-modal anti-tumor drug delivery system in the biomedical field.

Conflict of interest

The authors have declared no conflict of interest.

Acknowledgements

References

[1] Z. Bao, X. Liu, Y. Liu, H. Liu, K. Zhao, Near-infrared light-responsive inorganic nanomaterials for photothermal therapy, Asian. J. Pharm. Sci. 11 (2016) 349-364.

[2] A. Zhang, A. Li, Z. Wei, G. Yan, B. Liu, M. Liu, M. Li, B. Huo, J. Liu, An efficient and self-

guided chemo-photothermal drug loading system based on copolymer and transferrin decorated MoS$_2$ nanodots for dually controlled drug release, Chem. Eng. J. 342 (2018) 120-132.

[3] A. Zhang, A. Li, W. Tian, Z. Li, C. Wei, Y. Sun, W. Zhao, M. Liu, J. Liu, A target-directed chemo-photothermal system based on transferrin and copolymer-modified MoS$_2$ nanoplates with pH-activated drug release, Chem. Eur. J. 23 (2017) 11346-11356.

[4] J. Lee, J. Kim, W.J. Kim, Photothermally controllable cytosolic drug delivery based on core-shell MoS$_2$-porous silica nanoplates, Chem. Mater. 28 (2016) 6417–6424.

[5] W. Yin, L. Yan, J. Yu, G. Tian, L. Zhou, X. Zheng, X. Zhang, Y. Yong, J. Li, Z. Gu, Y. Zhao, High-throughput synthesis of single-layer MoS$_2$ nanosheets as a near-infrared photothermal-triggered drug delivery for effective cancer therapy, ACS Nano 8 (2014) 6922-6933.

[6] F. Yan, W. Duan, Y. Li, H. Wu, Y. Zhou, M. Pan, H. Liu, X. Liu, H. Zheng, NIR-laser-controlled drug release from DOX/IR-780-loaded temperature-sensitive-liposomes for chemo-photothermal synergistic tumor therapy. Theranostics   6 (2016) 2337-2351.

[7] F. Gu, R. Langer, O.C. Farokhzad, Formulation/preparation of functionalized nanoparticles for in vivo targeted drug delivery, Methods Mol. Biol. 544 (2009) 589-598.

[8] A.A. Bhirde, B.V. Chikkaveeraiah, S. Avinash, N. Gang, A.J. Jin, K. Ankur, W. Zhe, P. Sachin, P. Vyomesh, A.M. Gorbach, Targeted therapeutic nanotubes influence the viscoelasticity of cancer cells to overcome drug resistance, ACS Nano 8 (2014) 4177-4189.

[9] S.P. Sherlock, S.M. Tabakman, L. Xie, H. Dai, Photothermally enhanced drug delivery by ultra-small multifunctional FeCo/Graphitic-shell nanocrystals, ACS Nano 5 (2011) 1505-1512.

[10] H. Liu, D. Chen, L. Li, T. Liu, L. Tan, X. Wu, F. Tang, Multifunctional gold nanoshells on silica nanorattles: a platform for the combination of photothermal therapy and chemotherapy with low

systemic toxicity, Angew. Chem. Int. Ed. 50 (2011) 891-895.

[11] J.T. Robinson, S.M. Tabakman, Y. Liang, H. Wang, H.S. Casalongue, D. Vinh, H. Dai, Ultrasmall reduced graphene oxide with high near-infrared absorbance for photothermal therapy, J. Am. Chem. Soc. 133 (2011) 6825-6831.

[12] Q. Tian, M. Tang, Y. Sun, R. Zou, Z. Chen, M. Zhu, S. Yang, J. Wang, J. Wang, J. Hu, Hydrophilic flower-like CuS superstructures as an efficient 980 nm laser-driven photothermal agent for ablation of cancer cells, Adv. Mater. 23 (2011) 3542-3547.

[13] J. Wu, G.R. Williams, S. Niu, F. Gao, R. Tang, L.M. Zhu, A multifunctional biodegradable nanocomposite for cancer theranostics, Adv. Sci. 6 (2019) 1802001.

[14] H.K. Moon, S.H. Lee, H.C. Chol, In vivo near-infrared mediated tumor destruction by photothermal effect of carbon nanotubes, ACS Nano 3 (2009) 3707-3713.

[15] K. Yang, H. Xu, L. Cheng, C. Sun, J. Wang, Z. Liu, In vitro and in vivo near-infrared photothermal therapy of cancer using polypyrrole organic nanoparticles, Adv. Mater. 25 (2013) 5586-5592.

[16] H. Gong, L. Cheng, J. Xiang, H. Xu, L. Feng, X. Shi, Z. Liu, Near-infrared absorbing polymeric nanoparticles as a versatile drug carrier for cancer combination therapy, Adv. Funct. Mater. 23 (2013) 6059-6067.

[17] S. Wang, Z. Teng, P. Huang, D. Liu, Y. Liu, Y. Tian, J. Sun, Y. Li, H. Ju, X. Chen, G. Lu, Photothermal therapy: reversibly extracellular pH controlled cellular uptake and photothermal therapy by PEGylated mixed-charge gold nanostars, Small 11 (2015) 1738-1738.

[18] J. Wu, D.H. Bremner, S. Niu, H. Wu, J. Wu, H. Wang, H. Li, L.M. Zhu, Functionalized MoS_2 nanosheet-capped periodic mesoporous organosilicas as a multifunctional platform for synergistic

targeted chemo-photothermal therapy, Chem. Eng. J. 342 (2018) 90-102.

[19] T. Liu, C. Wang, X. Gu, H. Gong, L. Cheng, X. Shi, L. Feng, B. Sun, Z. Liu, Drug delivery with PEGylated MoS_2 nano-sheets for combined photothermal and chemotherapy of cancer, Adv. Mater. 26 (2014) 3433-3440.

[20] S. Gao, G. Tang, D. Hua, R. Xiong, J. Han, S. Jiang, Q. Zhang, C. Huang, Stimuli-responsive bio-based polymeric systems and their applications, J. Mater. Chem. B. 7 (2019) 709-729.

[21] W. Cheng, X. Zeng, H. Chen, Z. Li, W. Zeng, L. Mei, Y. Zhao, Versatile polydopamine platforms: synthesis and promising applications for surface modification and advanced nanomedicine, ACS Nano 13(2019) 8537-8565.

[22] Z. Wang, Y. Duan, Y. Duan, Application of polydopamine in tumor targeted drug delivery system and its drug release behavior, J. Control. Release. 290 (2018) 56-74.

[23] W. Tao, X. Ji, X. Zhu, L. Li, J. Wang, Y. Zhang, P.E. Saw, W. Li, N. Kong, M.A. Islam, T. Gan, X. Zeng, H. Zhang, M. Mahmoudi, G.J. Tearney, O.C. Farokhzad, Two-dimensional antimonene-based photonic nanomedicine for cancer theranostics, Adv. Mater. 30 (2018) 1802061.

[24] J. Kim, H. Kim, W.J. Kim, Single-layered MoS_2-PEI-PEG nanocomposite-mediated gene delivery controlled by photo and redox stimuli, Small 12 (2016) 1184-1192.

[25] Y. Liu, J. Liu, Hybrid nanomaterials of WS_2 or MoS_2 nanosheets with liposomes: biointerfaces and multiplexed drug delivery, Nanoscale 9 (2017) 13187-13194.

[26] S. Wang, Y. Chen, X. Li, W. Gao, L. Zhang, J. Liu, Y. Zheng, H. Chen, J. Shi, Injectable 2D MoS_2-integrated drug delivering implant for highly efficient NIR-triggered synergistic tumor hyperthermia, Adv. Mater. 27 (2015) 7117-7122.

[27] H. Yang, J. Zhao, C. Wu, C. Ye, D. Zou, S. Wang, Facile synthesis of colloidal stable MoS_2

nanoparticles for combined tumor therapy, Chem. Eng. J. 351 (2018) 548-558.

[28] X. Dong, W. Yin, X. Zhang, S. Zhu, X. He, J. Yu, J. Xie, Z. Guo, L. Yan, X. Liu, Intelligent MoS$_2$ nanotheranostic for targeted and Enzyme/pH/NIR-responsive drug delivery to overcome cancer chemotherapy resistance guided by PET Imaging, ACS Appl. Mater. Inter. 10 (2018) 4271-4284.

[29] P. Zhang, C. Hu, W. Ran, J. Meng, Q. Yin, Y. Li, Recent progress in light-triggered nanotheranostics for cancer treatment, Theranostics 6 (2016) 948-968.

[30] J. Shao, C. Ruan, H. Xie, Z. Li, H. Wang, P.K. Chu, X.F. Yu, Black-phosphorus-incorporated hydrogel as a sprayable and biodegradable photothermal platform for postsurgical treatment of cancer, Adv. Sci. 5 (2018) 1700848.

[31] X. Zhang, J. Wu, G.R. Williams, S. Niu, Q. Qian, L.M. Zhu, Functionalized MoS$_2$-nanosheets for targeted drug delivery and chemo-photothermal therapy, Colloid. Surf. B, Biointerf. 173 (2018) 101-108.

[32] L. Zhang, D. Sheng, D. Wang, Y. Yao, K. Yang, Z. Wang, L. Deng, Y. Chen, Bioinspired multifunctional Melanin-Based nanoliposome for photoacoustic/magnetic resonance imaging-guided efficient photothermal ablation of cancer, Theranostics 8 (2018) 1591-1606.

[33] G.N. Stamatas, B.Z. Zmudzka, K. Nikiforos, J.Z. Beer, Non-invasive measurements of skin pigmentation in situ, Pigment Cell Res. 17 (2010) 618-626.

[34] A.S. Elobeid, A. Kamal-Eldin, A. Mak, A.M. Haseeb, Pharmacological properties of melanin and its function in health, Basic Clin. Pharmacol Toxicol. 120 (2016) 515-522.

[35] M. Chu, H. Li, Q. Wu, F. Wo, D. Shi, Pluronic-encapsulated natural chlorophyll nanocomposites for in vivo cancer imaging and photothermal/photodynamic therapies, Biomaterials

35 (2014) 8357-8373.

[36] M. Chu, W. Hai, Z. Zhang, F. Wo, Q. Wu, Z. Zhang, Y. Shao, D. Zhang, L. Jin, D. Shi, Melanin nanoparticles derived from a homology of medicine and food for sentinel lymph node mapping and photothermal invivo cancer therapy, Biomaterials 91 (2016) 182-199.

[37] Q. Jiang, Z. Luo, Y. Men, P. Yang, H. Peng, R. Guo, Y. Tian, Z. Pang, W. Yang, Red blood cell membrane-camouflaged melanin nanoparticles for enhanced photothermal therapy, Biomaterials 143 (2017) 29-45.

[38] D. Zheng, S. Hong, L. Xu, C. Li, K. Li, S. Cheng, X. Zhang, Hierarchical micro-/nanostructures from human hair for biomedical applications, Adv. Mater. 27 (2018) 1800836.

[39] Q. Fan, K. Cheng, X. Hu, X. Ma, R. Zhang, M. Yang, X. Lu, L. Xing, W. Huang, S.S. Gambhir, Z. Cheng, Transferring biomarker into molecular probe: melanin nanoparticle as a naturally active platform for multimodality imaging, J. Am. Chem. Soc. 136 (2014) 15185-15194.

[40] C. Feng, Y. Han, H. Guo, X. Ma, Z. Wang, L. Wang, W. Zheng, J. Jiang, Self-assembling HA/PEI/dsRNA-p21 ternary complexes for CD44 mediated small active RNA delivery to colorectal cancer, Drug Deliv. 24 (2017) 1537-1548.

[41] H. Wang, J. Zhang, Y. Liu, T. Luo, X. He, X. Yu, Hyaluronic acid-based carbon dots for efficient gene delivery and cell imaging, RSC Adv. 7 (2017) 15613-15624.

[42] G. Jiang, K. Park, J. Kim, K.S. Kim, S.K. Hahn, Target specific intracellular delivery of siRNA/PEI−HA complex by receptor mediated endocytosis, Mol. Pharm. 6 (2009) 727-737.

[43] Y. Zhong, J. Zhang, R. Cheng, C. Deng, F. Meng, F. Xie, Z. Zhong, Reversibly crosslinked hyaluronic acid nanoparticles for active targeting and intelligent delivery of doxorubicin to drug resistant CD44+ human breast tumor xenografts, J. Control. Release. 205 (2015) 144-154.

[44] N. Yu, Y. Hu, X. Wang, G. Liu, Z. Wang, Z. Liu, Q. Tian, M. Zhu, X. Shi, Z. Chen, Dynamically tuning near-infrared-induced photothermal performances of TiO_2 nanocrystals by Nb-doping for imaging guided photothermal therapy of tumors, Nanoscale 26 (2017) 9148-9159.

[45] H. Lin, J. Wang, Q. Luo, H. Peng, C. Luo, R. Qi, R. Huang, J. Travas-Sejdic, C.G. Duan, Rapid and highly efficient chemical exfoliation of layered MoS_2 and WS_2, J. Alloy Compd. 699 (2017) 222–229.

[46] X. Yang, W. Fu, W. Liu, J. Hong, Y. Cai, C. Jin, M. Xu, H. Wang, D. Yang, H. Chen, Engineering crystalline structures of two-dimensional MoS_2 sheets for high-performance organic solar cells, J. Mater. Chem. A. 2 (2014) 7727-7733.

[47] Y. Li, H. Wang, L. Xie, Y. Liang, G. Hong, H. Dai, MoS_2 nanoparticles grown on graphene: an advanced catalyst for the hydrogen evolution reaction, J. Am. Chem. Soc. 133 (2011) 7296-7299.

[48] T. Antonio, A.M. Manuel, I. Pablo, E.M. Villar-Alvarez, B. Silvia, J.A. Costoya, T. Pablo, M. Víctor, Fluorescent drug-loaded, polymeric-based, branched gold nanoshells for localized multimodal therapy and imaging of tumoral cells, ACS Nano 8 (2014) 2725-2738.

[49] N. Lu, P. Huang, W. Fan, Z. Wang, Y. Liu, S. Wang, G. Zhang, J. Hu, W. Liu, G. Niu, Tri-stimuli-responsive biodegradable theranostics for mild hyperthermia enhanced chemotherapy, Biomaterials 126 (2017) 39-48.